# NMR Structure of α-Bungarotoxin Free and Bound to a Mimotope of the Nicotinic Acetylcholine Receptor†

Maria Scarselli,‡ Ottavia Spiga,‡ Arianna Ciutti,‡ Andrea Bernini,‡ Luisa Bracci,‡ Barbara Lelli,‡ Luisa Lozzi,‡ Duccio Calamandrei,§ Daniela Di Maro,§ Samuel Klein,‡ and Neri Niccolai*,‡

*Department of Molecular Biology and Biomolecular Structure Research Center, University of Siena, Siena, Italy, and BIOMODEM pscrl, Via Fiorentina 1, 53100 Siena, Italy*

*Received May 17, 2001; Revised Manuscript Received November 5, 2001*

Ⓦ **This paper contains enhanced objects available on the Internet at http://pubs.acs.org/biochemistry.**

ABSTRACT: A combinatorial library approach was used to produce synthetic peptides mimicking the snake neurotoxin binding site of nicotinic receptors. Among the sequences, which inhibited binding of α-bungarotoxin to muscle and neuronal nicotinic receptors, HRYYESSLPWYPD, a 14-amino acid peptide with considerably higher toxin-binding affinity than the other synthesized peptides, was selected, and the structure of its complex with the toxin was analyzed by NMR. Comparison of the solution structure of the free toxin and its complex with this peptide indicated that complex formation induced extensive conformational rearrangements mainly at finger II and the carboxy terminus of the protein. The peptidyl residues P10 and Y4 seemed to be critical for peptide folding and complex stability, respectively. The latter residue of the peptide strongly interacted with the protein by entering a small pocket delimited by D30, C33, S34, R36, and V39 toxin side chains.

Snake curaremimetic neurotoxins have very high affinity for nicotinic receptors (nAchR)[1] and produce a potent receptor functional blockade at neuromuscular junctions. Snake neurotoxins can be divided into two subfamilies: short (60−62 residues) and long (64−74 residues), which have a significant sequence homology and share the same three-dimensional structure. X-ray crystallography and NMR (for review, see refs *1* and *2*) show that they are composed of a globular core and three protruding loops. Short and long neurotoxins, including α-bungarotoxin (α-bgt), compete with acetylcholine and other nicotinic agonists and antagonists for binding to the receptor ligand site. Because of their high affinity and specificity, snake neurotoxins have been extremely useful in the characterization of nicotinic receptor structure and function.

This receptor is a complex pentameric molecule, whose high-resolution structure has not yet been determined. Functional studies have mapped the nAch binding site in the 181−200 region of the α-subunit, whereas α-bgt recognizes an overlapping fragment, spanning positions 173 to 204 (for review, see ref *3*).

Electron microscopy shows that the whole receptor has a cylindrical form, about 120 Å long, in which extracellular, transmembrane, and cytoplasmic parts can be recognized (*4*, *5*). It has been suggested that the Ach binding site is formed by juxtaposition of three extracellular alpha helices of the α subunits.

Most structural investigations on the interaction between nAchR and α-bgt have been performed by reproducing the region of nAchR involved in toxin binding. The NMR structure of the complex formed by α-bgt and the 185−196 fragment of *Torpedo californica* nAchR α1 subunit has been solved (*6*). This peptide, which has a $K_d$ of 1.4 $\mu$M, represents the first attempt to reproduce the nAchR binding site for the toxin in a synthetic smaller peptide. The three-dimensional structure of the complex reveals that the peptide binds to α-bgt in an extended conformation, between the first and second finger of the protein.

A phage library-derived peptide (LLPeP) having the sequence MRYYESSLKSYPD is reported to have a better affinity for α-bgt (*7*). The $IC_{50}$ of LLPep was $3.3 \times 10^{-7}$ M, and the NMR structure of the its complex with α-bgt indicated a very different type of peptide−toxin interaction (*8*). LLPeP folded in a globular conformation inside the toxin pocket formed by fingers I and II and the carboxy terminus moiety, establishing a hydrogen bond network involving residues $^{2}R_{LLPeP}-^{8}L_{LLPeP}$. LLPeP has an amino acid sequence very similar to the 187−200 AchR region of *Torpedo* α1 subunit.

† N.N. thanks the Italian MURST (PRIN 1999 and 2001) and the University of Siena for financial supports. L.B. thanks the Italian Murst (PRIN 1999) and the Italian CNR (PF Biotecnologie).

* To whom correspondence should be addressed. Neri Niccolai: phone, 0577 234910; fax, 0577 234903; e-mail, niccolai@unisi.it.

‡ University of Siena.

§ BIOMODEM.

[1] Abbreviations: α-bgt, α-bungarotoxin; BMRB, BioMagResBank; Fmoc, fluorenylmethoxycarbonyl; HOBt, *N*-hydroxybenzotriazole; HAPeP, phage library-derived peptide with sequence WRYYESSLKPYPD; HPLC, high performance liquid chromatography; NMR, nuclear magnetic resonance; NOE, nuclear Overhauser effect, NOESY, nuclear Overhauser enhancement and exchange spectroscopy; nAchR, nicotinic acetylcholine receptor; p6.7, 14-mer peptide with sequence HRYYESSLPWYPD; pdb, protein data bank; LLPeP, phage library-derived peptide with sequence MRYYESSLKSYPD; RMD, restrained molecular dynamics; RMSD, root-mean-square deviation; TOCSY, total correlation spectroscopy; $^{n}X_{\alpha-bgt}$, generic amino acid of α-bungarotoxin; $^{n}X_{p6.7}$, generic amino acid of HRYYESSLPWYPD.

10.1021/bi011012f CCC: $22.00 
Published on Web 01/11/2002

The peptide described in the present paper, a 14-mer with the sequence HRYYESSLEPWYPD, henceforth called p6.7, was selected by a semi-combinatorial approach. To build the synthetic peptide combinatorial library, amino acids in position 4, 12, and 14, representing residues conserved in α nAchr subunits from human, rat, mouse, and *Torpedo marmorata*, were kept invariant. C192 and C193, conserved in the cognate receptor sequences, were replaced by serine, and different amino acids were substituted in positions 2, 3, 5, and 13, using the sequence alignment of the different α nAchr subunits as guideline. Finally, peptide fine affinity tuning was achieved by systematic replacement of positions 1, 8, 9, 10, and 11 (*11*).

During the revision of this paper, the interaction of the new phage library-derived peptide WRYYESSLEPYPD, HAPeP, exhibiting a much higher α-bgt binding affinity, was presented (*9*). The structure and activity of the complex of HAPeP with the toxin were also related to its similarity to the amino-terminal ligand-binding domain of an nAChR α-subunit (*10*). Since LLPep, p6.7, and the latter AchR fragment contain the YY and YXD signatures, these residues presumably confer high α-bgt affinity.

The solution structure of α-bgt and its complex with the peptide p6.7 is investigated here by two-dimensional proton NMR spectroscopy. Structural results and α-bgt affinity of peptide p6.7, also with respect to other similar reported complexes (*7*−*9*, *11*), are discussed.

## MATERIALS AND METHODS

*Peptide Synthesis.* Solid-phase synthesis of p6.7 peptide was carried out with a MultiSynTech Syro automatic peptide synthesizer (Bochum, Germany) employing Fmoc chemistry with HOBt/DIC activation on a 4-(2′-4′-dimethoxyphenyl-Fmoc-aminomethyl)-phenoxyacetamido-norleucyl-4 methylbenzhydrylamine resin. Side chain protecting groups were as follows: *tert*-butyl ester for D and E; trityl for H, N, and Q; *tert*-butoxycarbonyl for K and W; 2,2,4,6,7-pentamethyldihydrobenzofuran-5-sulfonyl for R; and *tert*-butyl ether for S, T, and Y. The peptides were cleaved from the resins and deprotected by treatment with trifluoroacetic acid containing ethandithiol, water, triisobutylsilane, and anisole (93/2.5 /2/1.5/ 1). After precipitation of the sample with ethylic ether, the crude peptides were purified by preparative HPLC using a Vydac C-18 column (25 cm × 1 cm, 10 $\mu$m) and characterized by amino acid analysis and mass spectrometry.

*NMR Spectroscopy.* α-bgt was purchased from Calbiochem and used without further purification. The α-bgt/p6.7 complex, with a 1:1 stoichiometry, was prepared in 90% $H_2O$/10% $D_2O$, at a concentration of 0.5 mM and pH 5.7. $^1H$ NMR spectra of α-bgt, free and bound to p6.7, were acquired at 303 K using a Bruker Avance 600 spectrometer equipped with a Silicon Graphics Indy workstation.

TOCSY experiments with a mixing time of 75 ms were carried out to assign the resonances in each spin system. NOESY spectra at mixing times of 100, 120, and 150 ms were then acquired on the complex sample for the sequence-specific assignment and detection of dipolar couplings. Water suppression was achieved by WATERGATE (WATER suppression by GrAdient-Tailored Excitation) scheme (*12*). All 2D spectra were acquired with 2048 complex data points in t2 and 512 data points in t1, with a spectral width of 14 ppm. A 90-degree shifted sine-bell function was applied in both dimensions. All the spectra were processed with XWinNMR software (version 2.1, Bruker Inc.) and analyzed with NMRView (version 4.1.1) (*13*). The cross-peak intensities of NOESY spectra, at the different mixing times, were compared to eliminate the possibility of spin diffusion effects. The values obtained from the NOESY spectrum acquired at 150 ms of mixing time were used for structure calculation.

*Molecular Modeling.* NOEs intensities were translated into distance constraints using CALIBA (*14*). One hundred structures were generated for free and p6.7 peptide-bound α-bgt by a distance geometry-simulated annealing protocol with the version 1.5 of DYANA software (*15*), running on a Silicon Graphics R4400 workstation. The AMBER 4.1 force-field (*16*) was employed to simulate the α-bgt/p6.7 complex, using the united atom approximation. The whole system was surrounded by a sphere of Monte Carlo TIP3P waters and energy minimized for 500 steps with conjugate gradients, until the root-mean-square gradient of the potential energy was less than 0.02 kJ $mol^{-1}$ $nm^{-1}$. The refined coordinates were then used as starting point for 80 ps of restrained molecular dynamics (RMD) simulation at constant temperature. Initial velocities were taken from a Maxwellian distribution at $T_0 = 300$ K. The system was coupled to a heat bath at 300 K with a temperature relaxation time of 0.2 ps. All bond lengths were constrained at their equilibrium values using the SHAKE (*17*) algorithm, resetting the coordinates within a geometrical tolerance of 50 fm. To accelerate the calculation, the nonbonded pairs list was updated every 25 steps. Structures, energies, and velocities were saved every 100 steps (0.2 ps) throughout the 80 ps. Evolution of the complex was then monitored for an additional 80 ps of unrestrained molecular dynamics under the same conditions as for the RMD run. Hydrogen bonds were defined on the average minimized structures on the basis of donor−acceptor distances between 2.2 and 3.3 Å and a bond angle higher than 120°. All displays of structures, as well as exposed surface area (ESA) calculations, were carried out with the program MOLMOL (*18*).

## RESULTS

All the proton resonances of the toxin and the peptide in the free and bound forms were identified by standard assignment procedures. The chemical shifts of each hydrogen in the complex are reported in Tables 1 and 2.

*Structural Determination of α-bgt.* The chemical shift spread observed for the toxin was consistent with the presence of folded, mainly extended, secondary structure elements in solution. Information on the conformational stability of the protein was inferred from the extended network of the Overhauser effects. Of the 1096 dipolar connectivities measured, 368 were long range, i.e., arising from protons more than four residues distant in the sequence. These NOEs were, therefore, a reasonable set of experimental data for restrained molecular dynamics calculations. The good quality of our structure was confirmed by the calculated RMSD, which was 0.80 Å for backbone only and all heavy atoms in the 30 lowest energy structures.

*Structural Determination of Free p6.7.* The total absence of medium and long distance NOEs suggested that p6.7 was

Table 1: $^1$H Chemical Shifts[a] and Assignments of Free (plain) and Bound (bold) Forms of α-Bungarotoxin at pH 5.7, 30 °C

| Res | NH | $C^{\alpha}H$ | $C^{\beta}H$ | $C^{\gamma}H$ | others |
|---|---|---|---|---|---|
| **I1** | n.o.[c] | 4.15 **(4.16)** | 1.85 **(1.83)** | 1.16−1.55 **(1.15−1.56)**; 0.89 **(0.86)** | $C^{\delta}H_3$0.71 **(0.70)** |
| **V2** | 8.12 **(8.08)** | 4.96 **(4.98)** | 1.54 **(1.54)** | 0.55−0.84 **(0.55−0.84)** | |
| **C3** | 8.77 **(8.75)** | 5.04 **(5.06)** | 2.42−2.97 **(2.43−2.99)** | | |
| **H4** | 9.14 **(9.18)** | 5.03 **(5.05)** | 2.63−2.91 **(2.50−2.86)** | | |
| **T5** | 9.08 **(9.01)** | 5.17 **(5.24)** | 3.99 **(3.98)** | 1.30; 6.30 **(1.35; 6.34)** | |
| **T6** | 8.18 **(8.17)** | 4.75 **(4.45)** | 5.03 **(5.21)** | 1.42; 6.63 **(1.04; 6.73)** | |
| **A7** | 9.31 **(9.38)** | 4.32 **(4.50)** | 1.53 **(1.36)** | | |
| **T8** | 7.05 **(7.15)** | 4.49 **(4.52)** | 4.28 **(3.99)** | 1.03 **(1.03;7.00)** | |
| **S9** | 8.28 **(8.28)** | 4.58 **(4.77)** | 3.77−3.86 **(3.77−3.77)** | | |
| **P10** | | 4.86 **(5.00)** | 2.13−2.50 **(2.23−2.46)** | 1.81 **(1.77−1.96)** | $C^{\delta}H_2$ 3.58−3.58 **(3.54−3.74)** |
| **I11** | 8.43 **(8.71)** | 4.13 **(3.82)** | 1.68 **(1.46)** | 1.18−1.86 **(0.88−0.88)**; 1.04 **(0.30)** | $C^{\delta}H_3$ 0.90 (n.a.[d]) |
| **S12** | 7.77 **(7.58)** | 4.91 **(4.93)** | 3.77−3.87 **(3.82−3.82)** | | |
| **A13** | 8.25 **(8.21)** | 5.15 **(5.10)** | 0.89 **(0.87)** | | |
| **V14** | 8.86 **(8.87)** | 4.65 **(4.65)** | 2.07 **(2.24)** | 0.84 **(0.86)** | |
| **T15** | 8.48 **(8.49)** | 4.43 **(4.44)** | 3.99 **(4.01)** | 1.22 **(1.25)** | |
| **C16** | 8.86 **(8.83)** | 4.84 **(4.44)** | 2.97−3.34 **(2.98−3.36)** | | |
| **P17** | | 4.69 **(4.70)** | 1.77−2.40 **(1.76−2.41)** | 1.90−2.01 **(1.88−2.01)** | $C^{\delta}H_2$ 3.73−3.90 **(3.72−3.91)** |
| **P18** | | 4.28 **(4.28)** | 2.01−2.01 **(2.02−2.02)** | 1.87 **(1.85)** | $C^{\delta}H_2$ 3.58−3.86 **(3.57−3.88)** |
| **G19** | 8.74 **(8.75)** | 3.66−4.24 **(3.68−4.27)** | | | |
| **E20** | 7.83 **(7.86)** | 4.23 **(4.27)** | 2.09−2.09 **(2.12−2.12)** | 1.60−1.85 **(1.63−1.87)** | |
| **N21** | 7.76 **(7.79)** | 4.95 **(4.98)** | 2.65−2.98 **(2.66−2.99)** | | $N^{\delta}H_2$ 6.96−7.44 **(6.97−7.44)** |
| **L22** | 8.34 **(8.31)** | 4.98 **(4.98)** | 1.47−1.70 **(1.47−1.71)** | 1.57 **(1.58)** | $C^{\delta}H_3$ 0.70−0.77 **(0.72−0.77)** |
| **C23** | 8.75 **(8.73)** | 5.94 **(5.93)** | 2.84−3.24 **(2.84−3.22)** | | |
| **Y24** | 9.04 **(9.01)** | 5.97 **(6.02)** | 2.67−3.00 **(2.68−2.98)** | | $C^{\delta}H$ 6.64 **(6.66)**; $C^{\epsilon}H$ 6.76 **(6.74)** |
| **R25** | 9.05 **(9.01)** | 5.21 **(5.22)** | 1.33−1.90 **(1.33−1.88)** | 1.47 **(1.48)** | $C^{\delta}H_2$ 3.00 **(3.03)** |
| **K26** | n.a.[d] **(9.93)** | 5.83 **(5.22)** | 1.90−2.09 **(1.85−2.09)** | 1.58 **(1.54)** | $C^{\epsilon}H_2$ 2.57 **(2.54)** |
| **M27** | 9.22 **(9.20)** | 6.09 **(6.20)** | 2.03−2.48 **(1.93−2.00)** | 1.93−1.93 **(2.37−2.69)** | $SCH_3$ 1.97 **(1.98)** |
| **W28** | 8.56 **(7.95)** | 5.23 **(5.15)** | 3.44−3.75 **(3.46−3.68)** | | $C^{\eta}H$ 6.85 **(6.91)**; **$C^{\zeta}$H** 7.26 **(7.29)** $C^{\epsilon}H$ 7.53 **(7.44)**; $C^{\delta}H$ 7.04 **(6.91)** $N^{\epsilon}H$ 10.42 **(9.48)** |
| **C29** | 9.38 **(9.56)** | 5.14 **(5.36)** | 3.04−3.38 **(3.06−3.45)** | | |
| **D30** | 8.35 **(9.40)** | 4.87 **(4.96)** | 2.70−3.25 **(2.59−3.49)** | | |
| **A31** | 8.23 **(8.09)** | 4.04 **(4.04)** | 1.05 **(0.99)** | | |
| **F32** | 8.32 **(8.83)** | 4.82 **(4.96)** | 2.94−3.41 **(2.99−3.36)** | | |
| **C33** | 8.10 **(7.83)** | 4.13 **(4.27)** | 3.19−3.54 **(3.97−4.10)** | | |
| **S34** | 8.87 **(8.87)** | 4.28 **(4.19)** | 3.94−4.02 **(3.83−4.01)** | | |
| **S35** | 7.71 **(7.54)** | 4.66 **(4.73)** | 3.88−3.96 **(3.90−3.90)** | | |
| **R36** | 8.36 **(8.22)** | 4.57 **(4.62)** | 1.91−1.91 **(1.92−1.92)** | 1.65−1.78 **(1.76−1.76)** | $C^{\epsilon}H_2$ 3.08 **(2.72)**; $N^{\epsilon}H$ 7.05 **(7.18)** |
| **G37** | 7.67 **(7.47)** | 3.90−4.34 **(3.99−4.52)** | | | |
| **K38** | 8.18 **(9.67)** | 4.15 **(4.24)** | 1.45−1.60 **(1.51−1.71)** | 1.22 **(1.48)** | $C^{\epsilon}H_2$ 2.99 **(3.03)** |
| **V39** | 8.58 **(8.64)** | 3.57 **(3.51)** | 0.32 **(0.12)** | 0.47−0.54 **(0.25−0.34)** | |
| **V40** | 7.60 **(8.00)** | 4.68 **(4.46)** | 1.72 **(1.46)** | 0.52−0.52 **(0.46−0.58)** | |
| **E41** | 9.44 **(9.21)** | 4.98 **(5.08)** | 2.27−2.52 **(2.31−2.49)** | | |
| **L42** | 8.78 **(8.79)** | 5.07 **(4.86)** | 1.50 **(1.53)** | 1.56 **(1.59)** | $C^{\delta}H_3$ 0.74−0.84 **(0.74−0.84)** |
| **G43** | 6.75 **(6.72)** | 4.03−4.30 **(4.02−4.33)** | | | |
| **C44** | 8.46 **(8.44)** | 5.59 **(5.59)** | 3.17−3.35 **(3.18−3.37)** | | |
| **A45** | 9.30 **(9.30)** | 4.54 **(4.57)** | 1.39 **(1.40)** | | |
| **A46** | 8.77 **(8.75)** | 4.83 **(4.74)** | 1.51 **(1.52)** | | |
| **T47** | 7.40 **(7.39)** | 4.31 **(4.33)** | 3.93 **(3.94)** | 1.12 **(1.14)** | |
| **C48** | n.a.[d] **(9.01)** | 4.53 **(4.55)** | 2.90 **(2.90−3.22)** | | |
| **P49** | | 4.11 **(4.11)** | 1.51−2.07 **(1.52−2.09)** | 0.96−1.34 **(0.95−1.36)** | $C^{\delta}H_2$ 3.15−3.53 **(3.17−3.56)** |
| **S50** | 8.05 **(8.05)** | 4.19 **(4.16)** | 3.74−3.80 **(3.76−3.76)** | | |
| **K51** | 8.29 **(8.28)** | 4.40 **(4.42)** | 1.66−1.87 **(1.68−1.85)** | 1.46 **(1.47)** | $C^{\delta}H_2$ 1.25 **(1.31)**; $C^{\epsilon}H_2$ 3.09 **(3.09)** |
| **K52** | 8.69 **(8.66)** | 4.48 **(4.50)** | 0.82 **(0.86)** | 1.30 (n.a.[d]) | $C^{\delta}H_2$ 1.43−1.59 $C^{\epsilon}H_2$ 2.87 |
| **P53** | | 4.17 **(4.19)** | 1.76−2.23 **(1.78−2.20)** | 1.96 **(1.97)** | $C^{\delta}H_2$ 3.56−3.77 **(3.55−3.81)** |
| **Y54** | 7.00 **(7.07)** | 4.64 **(4.66)** | 3.12−3.47 **(3.15−3.53)** | | $C^{\delta}H$ **(6.79)**; $C^{\epsilon}H$ **(7.13)** |
| **E55** | 7.62 **(7.66)** | 5.06 **(5.04)** | 1.92−2.11 **(1.83−2.12)** | 1.79 **(1.82)** | |
| **E56** | 8.82 **(8.88)** | 4.76 **(4.79)** | 2.08−2.29 **(2.08−2.24)** | 1.99 **(2.00)** | |
| **V57** | 8.59 **(8.53)** | 5.35 **(5.27)** | 1.87 **(1.89)** | 0.88−0.91 **(0.86−0.96)** | |
| **T58** | 9.07 **(9.13)** | 4.75 **(4.75)** | 3.99 **(4.00)** | 1.22 (n.a.[d]) | |
| **C59** | 9.15 **(9.19)** | 5.62 **(5.63)** | 3.00−3.72 **(3.00−3.74)** | | |
| **C60** | 9.24 **(9.01)** | 5.11 **(5.13)** | 3.41−3.59 **(3.38−3.59)** | | |
| **S61** | 8.88 **(8.86)** | 4.93 **(4.96)** | 3.81−4.18 **(3.82−4.19)** | | |
| **T62** | 7.51 **(7.49)** | 4.75 **(4.75)** | 4.27 **(4.28)** | 1.20 **(1.21)** | |
| **D63** | n.a.[d] **(8.30)** | n.a.[d] **(4.81)** | 2.34−2.34 **(2.07−2.29)** | | |
| **K64** | n.a.[d] **(9.96)** | 3.16 **(3.15)** | 0.32−0.98 **(0.27−0.93)** | 1.48−1.50 **(1.45−1.45)** | $C^{\delta}H_2$ 1.49−1.53 **(1.71−1.71);** $C^{\epsilon}H_2$ 2.62−2.70 **(2.68−2.68)** |
| **C65** | 7.63 **(7.61)** | 4.55 **(4.56)** | 3.51−3.75 **(3.52−3.75)** | | |
| **N66** | 9.00 **(9.00)** | 4.97 **(5.28)** | 2.51−2.51 **(1.97−2.51)** | | $N^{\delta}H_2$ **(7.50−7.86)** |
| **P67** | | 3.64 **(3.61)** | 1.78−2.11 **(1.60−1.60)** | 1.63−1.81 **(1.73−1.73)** | $C^{\delta}H_2$ 3.46−3.63 **(3.58−3.58)** |
| **H68** | 8.38 **(8.53)** | 4.07 **(3.99)** | 2.77−2.86 **(2.65−2.65)** | | $C^{\delta}H$ 6.99 **(6.33)**; $C^{\epsilon}H$ 8.50 **(7.17)** |
| **P69** | | 4.32 **(4.30)** | 1.81−2.20 **(2.17−2.34)** | 1.90 **(2.08)** | $C^{\delta}H_2$ 2.66−3.32 **(3.19−3.19)** |
| **K70** | n.a.[d] **(11.12)** | 4.38 **(4.30)** | 1.77−1.92 **(1.78−2.01)** | 1.45 **(1.45)** | $C^{\delta}H_2$ 1.65 **(1.62)**; $C^{\epsilon}H_2$ 2.97 **(3.03)** |

Table 1 (Continued)

| Res | NH | $C^{\alpha}H$ | $C^{\beta}H$ | $C^{\gamma}H$ | others |
|---|---|---|---|---|---|
| **Q71** | 8.10 **(8.31)** | 4.24 **(4.28)** | 2.02−2.22 **(2.18−2.22)** | 1.92 **(1.95)** | $N^{\delta}H_2$ **(6.11−7.39)** |
| **R72** | 8.24 **(8.21)** | 4.60 **(4.60)** | 1.66−1.73 **(1.71−1.71)** | 1.84 **(1.87)** | $C^{\delta}H_2$ 3.20 **(3.21);** $N^{\epsilon}H$ 7.16 |
| **P73** | | 4.43 **(4.48)** | 2.04−2.25 **(2.01−2.26)** | 1.97 (n.a.[d]) | $C^{\delta}H_2$ 3.66−3.78 **(3.68−3.82)** |
| **G74** | 7.93 **(7.94)** | 3.75 **(3.69−3.85)** | | | |

[a] Chemical shifts in ppm; accuracy ± 0.01 ppm. [b] BMRB accession number 5006 for free α-bgt and 4849 for bound α-bgt. [c] n.o., not observed. [d] n.a., not assigned.

Table 2: $^{1}H$ Chemical Shifts[a] and Assignments of Free (plain) and Bound (bold) Forms of p6.7 at pH 5.7, 30 °C

| Res | NH | $C^{\alpha}H$ | $C^{\beta}H$ | $C^{\gamma}H$ | others |
|---|---|---|---|---|---|
| **H1** | n.o.[b] | 4.65 **(4.73)** | 3.24 **(3.23)** | | $C^{\delta}H$ 7.53 **(7.53)**; $C^{\epsilon}H$ **(7.70)** |
| **R2** | 8.06 **(8.07)** | 4.33 **(4.21)** | 1.61 **(1.60)** | 1.46 **(1.41)** | $C^{\delta}H_2$3.08 **(3.08)**; $N^{\epsilon}H$ 7.08 **(7.08)**; $N^{\zeta}H$ 6.80 **(6.74)** |
| **Y3** | 7.63 **(7.65)** | 4.65 **(4.69)** | 2.63−2.93 **(2.68−2.98)** | | $C^{\delta}H$ 7.68 **(7.68)** |
| **Y4** | 8.08 **(8.10)** | 4.52 **(4.56)** | 2.60−2.67 **(2.68−2.68)** | | $C^{\delta}H$ 7.61 (n.a.[c]) |
| **E5** | 8.26 **(7.82)** | 4.23 **(4.28)** | 1.91−2.03 **(1.91−2.06)** | 2.23 **(2.24)** | |
| **S6** | 8.22 **(7.93)** | 4.43 **(4.32)** | 3.85−3.92 **(3.85−3.91)** | | |
| **S7** | 8.28 **(7.93)** | 4.41 **(4.32)** | 3.84−3.90 **(3.85−3.91)** | | |
| **L8** | 8.14 **(8.29)** | 4.35 **(4.44)** | 1.62 **(1.65)** | 1.44 (n.a.[c]) | $C^{\delta}H_3$ 0.83−0.89 **(0.86−0.93)** |
| **E9** | 8.01 **(8.12)** | 4.50 **(4.55)** | 1.77−1.86 **(1.82−1.82)** | n.a.[c] **(2.29)** | |
| **P10** | | 4.12 **(4.14)** | 2.20−2.20 **(2.21−2.21)** | 1.89 **(1.91)** | $C^{\delta}H_2$3.41−3.52 **(3.54−3.74)** |
| **W11** | 7.81 **(7.77)** | 4.52 **(4.61)** | 3.13−3.13 **(3.22−3.22)** | | $C^{\delta}H$ 6.98 (n.a.[c]); $C^{\eta}H$ 6.76 (n.a.[c]); $C^{\zeta}H$ 7.14 (n.a.[c]); $N^{\epsilon}H$ 8.24 **(8.29)** |
| **Y12** | 7.97 **(7.93)** | 4.50 **(4.62)** | 2.88−2.97 **(2.95−3.12)** | | $C^{\delta}H$ n.a.[c] **(7.12)** |
| **P13** | | 4.33 **(4.40)** | 1.95−2.15 **(1.98−2.18)** | 1.72 **(1.76)** | $C^{\delta}H_2$3.59−3.70 **(3.65−3.76)** |
| **D14** | 8.43 **(8.40)** | 4.48 **(4.55)** | 2.88−2.94 **(3.00−3.05)** | | |

[a] Chemical Shifts in ppm; accuracy ± 0.01 ppm. [b] n.o., not observed. [c] n.a., not assigned.

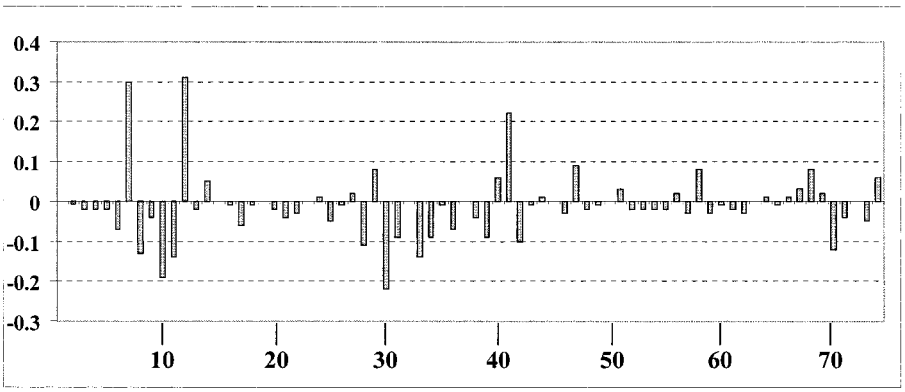


FIGURE 1: Histogram showing proton chemical shift variations observed for α hydrogens of α-bgt upon binding to the p6.7 peptide.

without conformational trend. Secondary signals due to the cis/trans conformational exchange at the $^{9}E_{p6.7}-^{10}P_{p6.7}$ peptide bond also confirmed that conformational equilibrium of the free peptide in solution was not shifted toward any predominant structure. These features were in line with the common conformational behavior of short linear peptides in water solution.

*Structural Determination of α-bgt/p6.7 Complex*. Preliminary chemical shift analysis provided information about residues most influenced by complex formation and about the dynamics of the protein−peptide interaction.

Peptide titration of the α-bgt solution at peptide/protein molar ratios of 1:4, 2:4, and 3:4 was performed to determine whether exchange conditions in solution were fast or slow. New signals of increasing intensity were produced, with a simultaneous decrease in intensity of others, ascribed to slow exchange conditions for the peptide−protein interaction (*19*) in agreement with previous results obtained by surface plasmon resonance (*11*). Furthermore, the total disappearance of some signals at a 1:1 molar ratio indicated a 1:1 stoichiometry for the complex.

Chemical shift changes of toxin and peptide α protons in their free and bound forms are shown in Figure 1. The α protons of $^{6}T_{\alpha-bgt}$, $^{11}I_{\alpha-bgt}$, and $^{40}V_{\alpha-bgt}$ clearly experienced a significant upper-field shift and $^{7}A_{\alpha-bgt}$, $^{10}P_{\alpha-bgt}$, $^{27}M_{\alpha-bgt}$, $^{29}C_{\alpha-bgt}$, and $^{70}K_{\alpha-bgt}$ showed an opposite behavior. Minor shifts (<0.1 ppm) were observed for $^{5}T_{\alpha-bgt}$, $^{28}W_{\alpha-bgt}$, $^{30}D_{\alpha-bgt}$, $^{33}C_{\alpha-bgt}$, $^{35}S_{\alpha-bgt}$, $^{38}K_{\alpha-bgt}$, $^{41}E_{\alpha-bgt}$, $^{46}A_{\alpha-bgt}$, and $^{57}V_{\alpha-bgt}$, suggesting weaker toxin−peptide interactions or minor conformational rearrangements on peptide binding.

NOESY spectra acquired for the 1:1 mixture of peptide and α-bgt yielded a set of 1606 distance restraints that were used for the structure calculations: 1475 and 74 corresponded to intramolecular protein and peptide NOEs, respectively, and 57 were derived from intermolecular protein−peptide dipolar connectivities. The large number of long-range NOEs, i.e., 759 and 27 for the protein and the peptide, respectively, provided a good basis for a restrained molecular dynamics calculation. Low RMSD of 0.55 and 0.77 Å, calculated for backbone only and all heavy atoms respectively, were obtained for the 20 lowest energy structures. The resulting

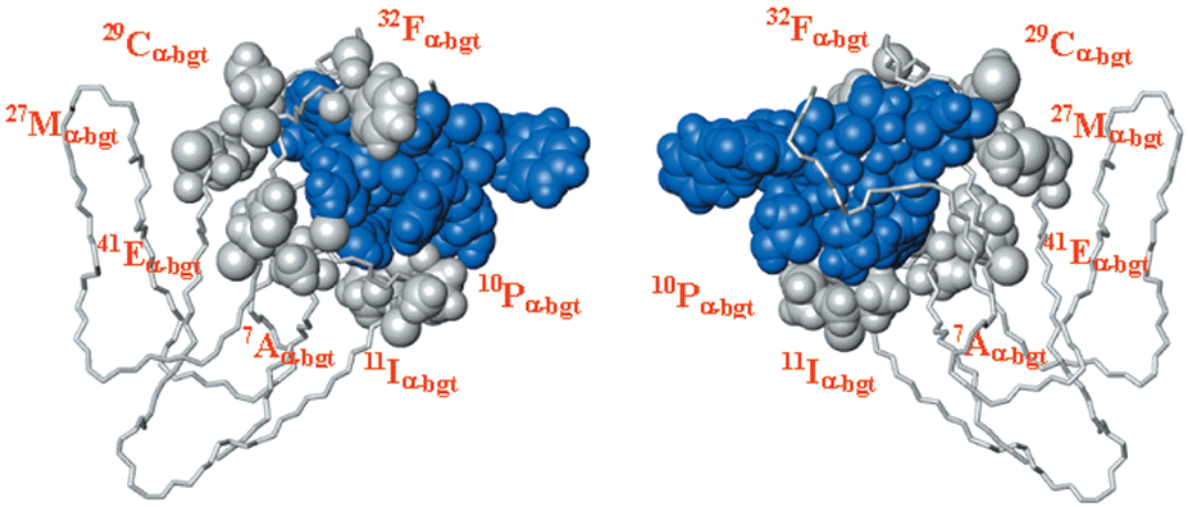


FIGURE 2: Complementary views of the α-bgt/p6.7 complex. The p6.7 peptide, as well as the α-bgt residues directly contacting the peptide, are shown in a space-fill representation, respectively, in blue and gray.

Table 3: Hydrogen Bonding Pattern of the Three Mimotope-α-bgt Complexes

| intermolecular H-bonds | | intramolecular H-bonds | |
|---|---|---|---|
| donor | acceptor | donor | acceptor |
| $V40NH_{\alpha-bgt}$ | $^{Y4}OH_{LLPeP}$ | $^{R2}NH_{LLPeP}$ | $^{Y11}CO_{LLPeP}$ |
| $^{Y3}NH_{LLPeP}$ | $^{V40}CO_{\alpha-bgt}$ | $^{Y11}NH_{LLPeP}$ | $^{R2}CO_{LLPeP}$ |
| $^{E5}NH_{LLPeP}$ | $^{K38}CO_{\alpha-bgt}$ | $^{S7}NH_{LLPeP}$ | $^{Y4}CO_{LLPeP}$ |
| | | $^{R2}NH_{LLPeP}$ | $^{D8}O\delta1_{LLPeP}$ |
| $^{D30}NH_{\alpha-bgt}$ | $^{Y4}OH_{HAPeP}$ | $^{S6}NH_{HAPeP}$ | $^{Y4}CO_{HAPeP}$ |
| $^{K38}NH_{\alpha-bgt}$ | $^{E5}O\epsilon_{HAPeP}$ | $^{Y4}NH_{HAPeP}$ | $^{R2}CO_{HAPeP}$ |
| $^{R2}N\zeta H1_{HAPeP}$ | $^{D30}O\delta1_{\alpha-bgt}$ | $^{Y4}NH_{HAPeP}$ | $^{Y11}OH_{HAPeP}$ |
| $^{R2}N\zeta H1_{HAPeP}$ | $^{D30}O\delta1_{\alpha-bgt}$ | | |
| $^{Y3}OH_{HAPeP}$ | $^{S9}CO_{\alpha-bgt}$ | | |
| $^{Y3}OH_{p6.7}$ | $^{S9}CO_{\alpha-bgt}$ | $^{H1}NH_{p6.7}$ | $^{D14}O\delta_{p6.7}$ |
| $^{R2}N\zeta H1_{p6.7}$ | $^{A7}CO_{\alpha-bgt}$ | $^{R2}N\delta H_{p6.7}$ | $^{Y3}OH_{p6.7}$ |
| $^{R2}N\zeta H2_{p6.7}$ | $^{A7}CO_{\alpha-bgt}$ | $^{E9}NH_{p6.7}$ | $^{S7}O\gamma_{p6.7}$ |
| $^{R2}N\epsilon H_{p6.7}$ | $^{D30}O\delta1_{\alpha-bgt}$ | $^{W11}NH_{p6.7}$ | $^{E9}CO_{p6.7}$ |
| $^{R2}N\zeta H_{p6.7}$ | $^{D30}O\delta1_{\alpha-bgt}$ | $^{Y12}NH_{p6.7}$ | $^{E9}CO_{p6.7}$ |
| $^{Y4}OH_{p6.7}$ | $^{D30}NH_{\alpha-bgt}$ | $^{Y3}OH_{p6.7}$ | $^{S9}CO_{p6.7}$ |
| $^{H1}N\epsilon H_{p6.7}$ | $^{S9}CO_{\alpha-bgt}$ | | |

three-dimensional structure of the α-bgt/p6.7 complex is shown in Figure 2. All residues with major α proton chemical shift changes formed a pocket around the bound p6.7 peptide.$^{6}T_{\alpha-bgt}$, $^{7}A_{\alpha-bgt}$, $^{10}P_{\alpha-bgt}$, $^{11}I_{\alpha-bgt}$, $^{27}M_{\alpha-bgt}$, $^{29}C_{\alpha-bgt}$, $40V_{\alpha-bgt}$, and $^{70}K_{\alpha-bgt}$ were located in a cavity of α-bgt formed by fingers I and II, and the C-terminal portion of the toxin. The conformation of the peptide in the toxin pocket consisted of a major loop from $^{4}Y_{p6.7}$ to $^{8}L_{p6.7}$, a slight bend at $^{9}E_{p6.7}-^{11}W_{p6.7}$, and a minor loop involving $^{12}Y_{p6.7}$, $^{13}P_{p6.7}$, and $^{14}D_{p6.7}$. The peptide structure was stabilized by six intramolecular and eight intermolecular hydrogen bonds, Table 3.

The conformation of p6.7 in the complex consisted of two consecutive bents, which maintained the peptide in a compact globular structure. $^{3}Y$ and $^{4}Y$ were the amino acids most directly involved in the interaction with α-bgt. $^{4}Y_{p6.7}$ entered a small pocket delimited by the side chains of $^{30}D_{\alpha-bgt}$, $^{33}C_{\alpha-bgt}$, $^{34}S_{\alpha-bgt}$, $^{36}R_{\alpha-bgt}$, and $^{39}V_{\alpha-bgt}$, so that its aromatic ring established a hydrophobic interaction with the aliphatic portion of $^{36}R_{\alpha-bgt}$ side and $^{39}V_{\alpha-bgt}$ gamma, see Figure 3.

## DISCUSSION

The solution structure of α-bgt and its interaction with a mimotope of nAchR were investigated on the basis of

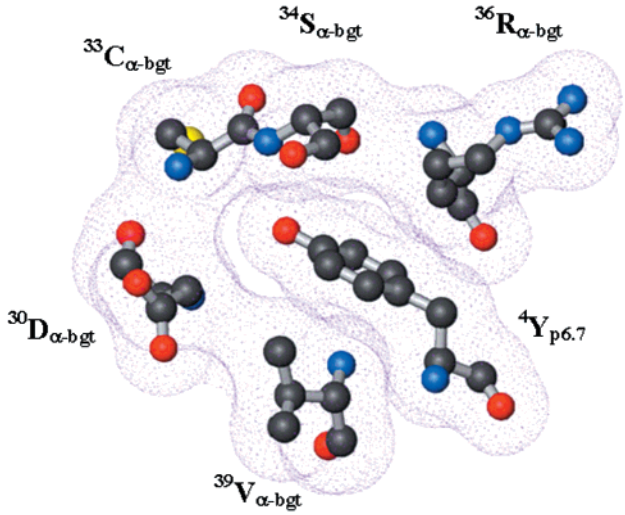


FIGURE 3: The critical role of the $^{4}Y_{p6.7}$ side chain in the docking with the α-bgt surface is highlighted.

Ⓦ An animated video in mpg format is available.

chemical shift changes and NOEs. Our structure of the free α-bgt is consistent to the one previously reported (*20*). In the complex with p6.7 peptide, the amino acids forming the binding site of the toxin could be clearly identified by the intermolecular NOE pattern, consistently with the observed α proton chemical shifts changes. The 5−12, 27−34, 38−42, and 70−74 segments of the protein are critical for the interaction with the peptide, and, interestingly, the same toxin regions are recognized by a single-chain Fv previously identified as an effective nAchr mimotope (*21*).

Correlations of peptide sequence, protein conformational changes, and complex affinity for p6.7/α-bgt can be discussed in the light of the two other AchR mimotopes/α-bgt complexes now available, i.e., LLPeP/α-bgt (*8*) and WRYYESSLEPYPD (HAPeP)/α-bgt (*9*). The protein−peptide affinity of the complexes formed by α-bgt with p6.7, LLPeP, and HAPeP, expressed as $IC_{50}$, was, respectively, $1.2 \times 10^{-7}$, $3.3 \times 10^{-7}$, and $2.0 \times 10^{-9}$ M. It is worth noting that the three peptides exhibited such a different binding strength despite their close similarity in length and amino acid composition. The structural basis of these features could be easily analyzed, as the Protein Data Bank files of the three

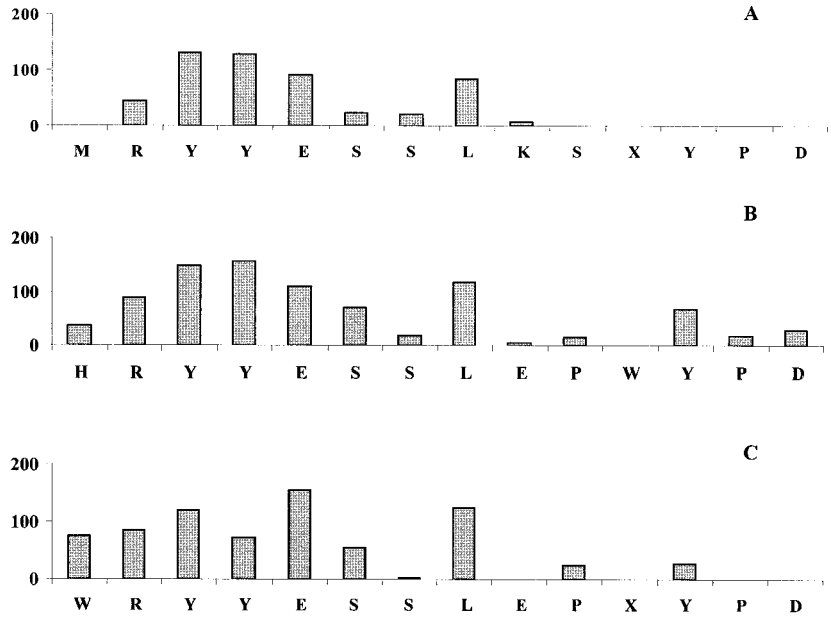


FIGURE 4: Comparison of intermolecular contacts between α-bgt and (A) LLPeP, (B) p6.7, and (C) HAPeP. Histogram heights refer to the contact areas of each residue, expressed in Å$^2$ and calculated by using a sphere of 1.4 Å of diameter as a probe.

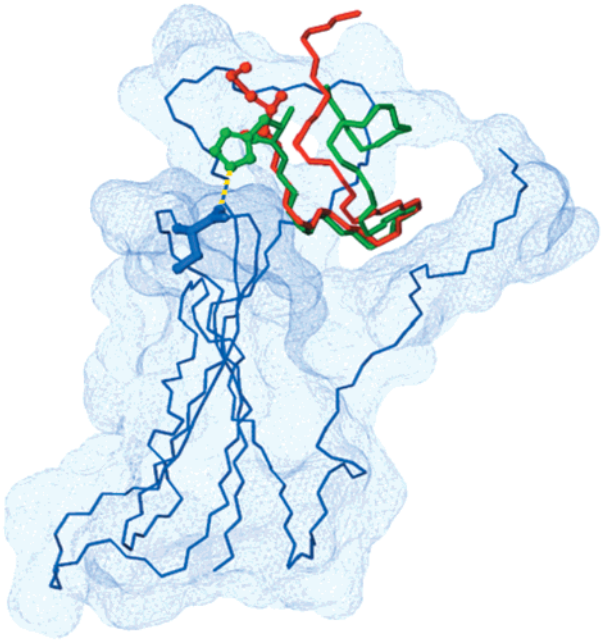

FIGURE 5: General overview of the three-dimensional structure of the complex α-bgt with p6.7 (green) and LLPeP (red), both inserted in the toxin active site according to the proposed structures. The two peptides have a backbone stick representation, apart from $^1H_{p6.7}$, $^1M_{LLPeP}$, and $^9S_{\alpha-bgt}$ whose side chains are shown as ball-and-sticks. The hydrogen bonding between the NHϵ of $^1H_{p6.7}$ and the carboxylic group of is highlighted.

α-bgt complexes are all web available (PDB id codes are the following: p6.7/α-bgt: 1JBD; LLPeP /α-bgt: 2BTX; HAPeP /α-bgt: 1HAA).

From a comparison of the positional parameters of backbone heavy atoms for the couples 1JBD−2BTX and 1JBD−1HAA of the common RYYESSL segment, very similar local conformations were found with RMSD of 0.15 and 0.66 Å, respectively. Larger conformational differences were found for the remaining part of the peptides and for the α-bgt regions involved in the binding. Table 4 summarizes the conformational changes occurring in the most relevant toxin moieties for the peptide binding. The protein carboxy terminus experiences the biggest change upon binding of p6.7, while finger II moves toward HAPeP more markedly than in the other two cases. During the complex formation, the largest conformational rearrangement was observed in the presence of p6.7. The latter complex, despite the longer sequence of the bound peptide, exhibited the smallest ESA, see Table 4. The W/H replacement at the amino terminus and the W insertion at position 11 determine a very compact structure for p6.7/α-bgt, when compared to the one of HAPep/α-bgt.

Table 4: Backbone Heavy Atoms RMSD Calculated from the Structure of the Free α-Bungarotoxin[a,b]

| | 1JBD | 1HAA | 2BTX |
|---|---|---|---|
| RMSD finger I$^{5-12}$ | 1.55 | 1.41 | 1.91 |
| RMSD finger II$^{28-39}$ | 1.65 | 2.41 | 1.63 |
| RMSD carboxy terminus$^{68-74}$ | 2.53 | 1.34 | 2.28 |
| overall RMSD | 4.68 | 4.00 | 4.35 |
| ESA | 4921 | 4994 | 4970 |
| peptide−protein contact area | 742 | 606 | 502 |
| no. long-range intraprotein NOEs | 759 | 245 | 291 |
| no. long-range intrapeptide NOEs | 27 | 12 | 7 |
| no. intermolecular NOEs | 57 | 92 | 62 |

[a] PDB code 1IK8. [b] Numbers in parenthesis refer to the considered fragments; overall exposed surface areas (ESA) of the complexes and peptide−protein contact areas are expressed in Å$^2$.

The interactions that α-bgt established with p6.7, LLPeP, and HAPeP could also be delineated by calculating contact area profiles between the protein and each peptide residue in the three complexes, see Figure 4. The overall exposed surface areas, ESA, of the three complexes was measured in the presence and in the absence of the bound peptides, yielding the protein−peptide contact areas reported in Table 4. Although these profiles were all comparable in the N-terminal portions, in the case of p6.7 an increase of contact area at the carboxy terminus could be observed. The $^{12}YPD^{14}_{p6.7}$ tripeptide, indeed, showed an overall contact area of 114.4 Å$^2$ with the toxin, mainly ascribed to $^{12}Y_{p6.7}$, while the last three amino acids of LLPeP and HAPeP did not

establish any relevant interaction with α-bgt. In agreement with the peptide size and the structural compactness of the complex, the highest contact area was found for p6.7. The intermolecular hydrogen bonding patterns of the three complexes, summarized in Table 3, were also very different. In the case of the 1HAA structure, there were only a few H-bonds, while in the 1JBD structure many H-bonds were found.

Some disagreement between structural features and affinity for the three complexes seemed to occur, if the dynamic aspects of the interaction were not taken into account. As already suggested (*9*), the formation of the $\beta$-hairpin regular conformation adopted by HAPeP inside the toxin complex, partially accounted for its observed high affinity. Furthermore, the fact that the smallest conformational changes with respect to the unbound toxin were induced by HAPeP, see Table 4, could reasonably determine the lowest $k_{off}$ for the HAPeP/α-bgt complex. This hypothesis was consistent with the NOE constraints found for the various complexes: a high number of intramolecular NOEs and only few intermolecular NOEs were measured for p6.7/α-bgt (see Table 4).

As a final remark, a central role in increasing the peptide/α-bgt complex affinity with respect to LLPeP/α-bgt seemed to be played by $^{10}P_{p6.7}$. In fact, although the prolyl residue was not directly in contact with the toxin, it could favor the peptide backbone to fold inside the α-bgt pocket (Figure 5).

## ACKNOWLEDGMENT

Thanks are due to Dr. F. Foglia, M. Bernardini, and I. Fiaschi for helpful discussions.

## REFERENCES

1. Endo, T., and Tamia N. (1987) *Pharmacol. Ther. Rev. 34*, 403−451.
2. Tsetlin, V. (1999) *Eur. J. Biochem. Rev. 264*, 281−286.
3. Arias, H. R. (1997) *Brain Res. Rev. 25*, 133−191.
4. Unwin, N. (1995) *Nature 373*, 37−43.
5. Unwin, N. (1996) *J. Mol. Biol. 257*, 586−596.
6. Basus, V. J., Guoqiang, S., and Hawrot, E. (1993) *Biochemistry 32*, 12290−12298.
7. Balass, M., Katchalski-Katzir, E., and Fuchs, S. (1997) *Proc. Natl. Acad. Sci. U.S.A. 94*, 6054−6058.
8. Scherf, T., Balass, M., Fuchs, S., Katchalski-Katzir, E., and Anglister, J. (1997) *Proc. Natl. Acad. Sci. U.S.A. 94*, 6059−6064.
9. Scherf, T., Kasher, R., Balass M., Fridkin M., Fuchs S., and Katchalski-Katzir, E. (2001) *Proc. Natl. Acad. Sci. U.S.A. 98(12)*, 6629−6634.
10. Brejc, K., van Dijk, W. J., Klaassen, R. V., Schuurmans, M., van Der Oost, J., Smit, A. B., and Sixma, T. K. (2001) *Nature 411(6835)*, 252−255.
11. Bracci L., Lozzi L., Lelli B., Pini A., and Neri, P. (2001) *Biochemistry 40(22)*, 6611−6619.
12. Piotto, M., Saudek, V., and Sklenar, V. (1992) *J. Biomol. NMR 2*, 661−666.
13. Johnson, B. A., and Blevins, R. A. (1994) *J. Biomol. NMR 4*, 603−614.
14. Guntert, P., Broun, W., and Wüthrich, K. (1991), *J. Mol. Biol. 217*, 517−530.
15. Guntert, P., Mumenthaler, C., and Wüthrich, K. (1997) *J. Mol. Biol. 273*, 283−298.
16. Cornell, W. D., Cieplak, P., Bayly, C. I., Gould, I. R., Merz, K. M., Jr., Ferguson, D. M., Spellmeyer, D. C., Fox, T., Caldwell, J. W., and Kollman, P. A. (1995) *J. Am. Chem. Soc. 117*, 5179−5197.
17. Van Gunsteren, W. F., and Berendsen, H. J. C. (1977) *Mol. Phys. 34*, 1311−1327.
18. Koradi, R., Billeter, M., and Wüthrich, K. 1996. *J. Mol. Graph. 14*, 51−55.
19. Craik, D. J., and Wilce, A. (1997) in *Methods in Molecular Biology 60* (Reid, D. G., Ed.) pp 195−232, Humana Press Inc., Totowa, NJ.
20. Zeng, H., Moise, L., Grant, M. A., and Hawrot, E. (2001) *J. Biol. Chem. 276*, 22930−22940.
21. Bracci, L., Pini, A., Lozzi, L., Lelli, B., Battestin, P., Spreafico, A., Bernini, A., Niccolai, N., and Neri P. (2001) *J. Neurochem. 78*, 24−31.

BI011012F